ACS EARTH AND SPACE CHEMISTRY

http://pubs.acs.org/journal/aesccq

Article

Ferrihydrite Transformation Impacted by Adsorption and Structural Incorporation of Rare Earth Elements

Meijun Yang, Xiaoliang Liang, Ying Li, Hongping He,* Runliang Zhu, and Yuji Arai*

Cite This: *ACS Earth Space Chem.* 2021, 5, 2768−2777

Read Online

ACCESS | Metrics & More | Article Recommendations | Supporting Information

ABSTRACT: Understanding the association of rare earth elements (REEs) with iron (oxyhydr)oxides is of great interest in the recovery of REEs from regolith and weathered soils in the world. The objective of this study was to understand the effects of 1 mg L^{-1} REEs on the ferrihydrite transformation process. Ferrihydrite was synthesized at pH 5 and 7 in the presence of REEs, and the transformation products were characterized using X-ray diffraction, Fe K-edge X-ray absorption spectroscopy, and transmission electron microscopy. During the phase transformation process after 60−120 days, the retention of REEs varied with the REE atomic number. In general, heavy REEs preferably partitioned in aged (≥90 days) ferrihydrite more than light REEs, especially at pH 5. At pH 5, the transformation of ferrihydrite to goethite was retarded by ∼12% when REEs were present. The average structural substitution of REEs was as high as ∼550 mg kg^{-1}, and the substitution of heavy REEs such as Yb and Lu was a critical factor to suppress the ferrihydrite transformation. At pH 7, the formation of hematite was retarded by ∼10%, and the structural incorporation of REEs was more important than adsorbed REEs during the first 30 days. There was no REE-specific retention in aged iron (oxyhydr)oxides at pH 7. The results of this study may explain the association of REEs with iron (oxyhydr)oxides, especially heavy REEs in mildly acidic regolith and weathered soils. This study advanced our understanding of the aqueous geochemical behavior of REEs in iron (oxyhydr)oxide-rich supergene environments.

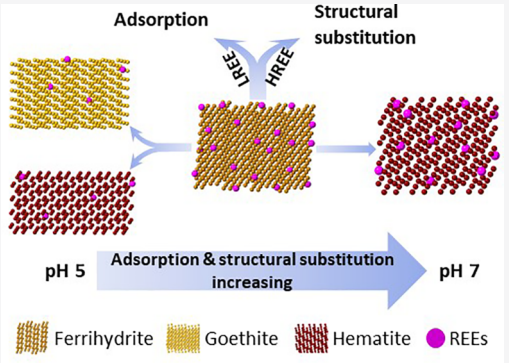

KEYWORDS: *rare earth element, ferrihydrite, hematite, goethite, transformation, adsorption, substitution*

INTRODUCTION

Rare earth elements (REEs) are a coherent suite of elements consisting of lanthanides as well as scandium (Sc) and yttrium (Y). REEs exist in a trivalent oxidation state, except for Ce and Eu, which are also stable under some conditions in tetra- and divalent oxidation states, respectively. Besides the difference in valence, REEs have slight variations in physical and chemical properties due to the lanthanide contraction effect, i.e., the decrease in ionic radii from La^{3+} (1.032 Å) to Lu^{3+} (0.861 Å) across the group. Both variations allow discrepancies among REEs (e.g., Ce and Eu anomalies),[1,2] light REEs (LREEs, La−Eu),[3] and heavy REEs (HREEs, Gd−Lu and Y) during natural geochemical processes.[3−7]

As the fourth most abundant element on Earth, iron is redox-active and ubiquitous as iron (oxyhydr)oxide minerals in suboxic to oxic soils, sediments, and regolith. Because of their reactive surface, they are effective in scavenging REEs, often resulting in the enrichment of REEs. Regolith-hosted REE deposits are dominantly located in the weathering crusts of granites and soils in South China, with a few deposits, and potential prospects recently discovered and explored in Southeast Asia,[8−11] Madagascar,[12] and the Southeastern United States.[13] The ore grades range from 140 to 6500 mg kg^{-1} (typically ∼800 mg kg^{-1}) of REEs, and some of the deposits are remarkably enriched in HREEs.[14] Iron (oxyhydr)oxides are ubiquitous in these deposits and are important sinks of REEs in weathered soils.[15−17] The sorption of REEs on iron (oxyhydr)oxides occurs over a wide range of pH.[18−20] As a redox-sensitive REE, Ce(III) can be oxidized after its adsorption on the iron (oxyhydr)oxide surface, contributing to the pronounced positive Ce anomaly, which is characteristic of marine hydrogenetic ferromanganese crusts.[21] Besides adsorption and oxidation, REEs can also coprecipitate with Fe during the weathering of granite[22] and structurally incorporate in iron (oxyhydr)oxides,[23] resulting in a higher removal of REEs than the adsorption on pre-exist iron (oxyhydr)oxides.[24]

Thus, understanding the fate of REEs in iron (oxyhydr)oxides is a major economic interest because the REE recovery technologies are dependent on their ion exchangeability and solubility in iron (oxyhydr)oxides. In the Fe geochemical cycle,

Received: May 25, 2021
Published: September 14, 2021

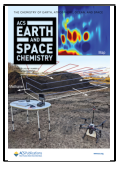

amorphous iron (oxyhydr)oxide (e.g., ferrihydrite) is a thermodynamically metastable phase that transforms into crystalline iron (oxyhydr)oxides (e.g., hematite and goethite) under (sub)oxic conditions. Along with phase transformation, various metal ions are often associated with ferrihydrite, leading to the variation of stability and mobility of metals in terrestrial environments. Aging studies of ferrihydrite with metals (e.g., Cd(II), Mn(II), Ni(II), and Pb(II)) showed that the transformation reactions were influenced by the structural incorporation of metals into recrystallized oxides.[25,26] A few studies showed that the phase transformation of ferrihydrite was also affected by adsorbed REEs (e.g., Lu(III)).[27,28] However, the mechanisms responsible for the suppressed ferrihydrite transformation by REEs are not clearly understood.

Based on the results of above discussions, it was hypothesized that the transformation products of ferrihydrite coprecipitated with REEs are REE specific. Considering the smaller difference of ionic radii with Fe(III), HREEs (e.g., Tb(III): 0.923 Å, Ho(III): 0.901 Å, and Lu(III): 0.861 Å) are easily incorporated within the structure of iron (oxyhydr)oxides than LREEs (e.g., La(III): 1.032 Å, Ce(III): 1.010 Å,, and Nd(III), 0.983 Å).[29,30] During the formation and transformation process of iron (oxyhydr)oxides, LREEs could be scavenged by ferrihydrite through adsorption. Accordingly, the objective of this study was to investigate the phase transformation products of ferrihydrite impacted by LREEs and HREEs using powder X-ray diffraction (XRD), transmission electron spectroscopy (TEM), and Fe K-edge X-ray absorption spectroscopy (XAS).

MATERIALS AND METHODS

Materials. All chemicals (e.g., $FeCl_3$, $Nd(NO_3)_3{\cdot}6H_2O$, and $Yb(NO_3)_3{\cdot}5H_2O$) (Sigma−Aldrich, St. Louis, MO) used were ACS grade. All the solutions were prepared with ultrapure water (18.25 MΩ cm^{-1}) under atmospheric conditions unless otherwise mentioned in the text. The mixed REE stock solution was obtained after diluting an 100 μg mL^{-1} inductively coupled plasma mass spectrometry (ICP-MS) standard solution containing La, Ce, Pr, Nd, Sm, Eu, Gd, Tb, Dy, Ho, Er, Tm, Yb, and Lu (AccuStandard, CT) except for Pm.

Synthesis of Iron (Oxyhydr)oxide with and without REEs. To investigate the partitioning of LREEs and HREEs during the transformation of iron (oxyhydr)oxides under atmospheric pressure, a group of REEs was mixed simultaneously with ferric chloride solution (500 mg L^{-1}). The Fe/REEs ratio of 100:3 was chosen to observe the effect of REEs on the ferrihydrite transformation. The concentration of each rare earth element was 1 mg L^{-1}, and the negative saturation index value for each REE hydroxide (Table S1), which was calculated using Visual MINTEQ version 3.1[31] and/or manually, suggested that REEs retained in ferrihydrite were either adsorbed and/or substituted in the structure. The mixture of Fe and REEs was titrated to pH 5 and 7 using 0.01−0.1 M NaOH. Brown suspensions were divided into perfluoroalkoxy bottles that give a duplicate sample for each sample period. Afterward, the bottles were sealed and stored in an oven at 40 °C for 60 days, but the experiments at pH 5 were carried out longer, up to 120 days, due to a slow transformation process. These aging times allowed each control system to transform ∼80% of ferrihydrite. The REE-blank control experiments were also conducted to monitor REE adsorption in the same reaction vessels at pH 5 and 7. The bottles were periodically shaken during aging. The pH was periodically adjusted with 0.1 M NaOH solution, with pH variations less than 0.1 units. Kinetic samples were recovered via centrifugation, while the dissolved concentrations of REEs and Fe in the supernatant were analyzed using inductively coupled plasma mass spectrometry (ICP-MS) (Thermo iCAPQc, Guangzhou, China). After washing solids with ultrapure water, the solids were freeze-dried and stored at room temperature for XRD and XAS analyses. Reference iron (oxyhydr)oxide standards (i.e., 2-line ferrihydrite, hematite, and goethite) were synthesized according to the method described by Schwertmann and Cornell.[32] The ferrihydrite without REEs was aged at pH 5 and 7 as a control experiment. These two pH values were chosen to simulate the environmentally relevant pH values in regolith and weathered soil profiles in Southern China.[14,33]

To estimate the amount of REE structural substitution, the following experiment was conducted. Approximately 5 mg of kinetic sample was exchanged with 20 mL of 1 M NH_4NO_3 at pH 5 (i.e., below isoelectric point, IEP of iron (oxyhydr)oxides) to remove adsorbed and diffused REEs in the solids. The mineral suspension was shaken on an orbital shaker at 90 rpm. After a few hours, the sample was centrifuged at 7500g for 20 min. The recovered mineral paste was digested in 1 mL of 6 M HCl, and an aliquot was analyzed for dissolved REEs using ICP-MS to estimate structurally incorporated REEs in iron (oxyhydr)oxides.

Powder X-ray Diffraction. The phase of iron (oxyhydr)oxides with and without REEs was analyzed using XRD. XRD patterns were acquired on a Rigaku DMAX Rapid II diffractometer with Mo Kα radiation at 50 kV and 30 mA with a 0.02° step size at a scan rate of 1° per second for analysis. Bulk solid products were ground to less than 200 mesh and then loaded into Kapton fiber tubes with a diameter of 0.3 mm. The two-dimensional data were converted to 2θ vs intensity patterns using Rigaku's 2DP software.

Transmission Electron Microscopy. The morphology of aged iron (oxyhydr)oxides coprecipitated with REEs (REE-Fe (oxyhydr)oxides) was investigated using a Thermo Scientific FEI Talos F200S transmission electron microscope (Guangzhou, China), operated at an accelerating voltage of 200 kV. The sonicated mineral suspensions in ultrapure water were deposited on a porous carbon film supported by a copper grid. Iron (oxyhydr)oxide phases were analyzed through selected area electron diffraction (SAED) patterns and from fast Fourier transforms (FFT) from high-resolution lattice-fringe images.

Fe K-Edge X-ray Absorption Spectroscopy. Because XRD is not sensitive to quantify amorphous phases such as ferrihydrite, Fe K-edge extended X-ray absorption fine structure spectroscopy (EXAFS) measurements were conducted on Beamline 12-BM at Advanced Photon Source (Argonne, IL). An aliquot of each freeze-dried sample was diluted with boron nitride at 5−10% by wt. The mixture was poured in a nylon washer that was sealed with Kapton tape. Measurements were performed at room temperature in transmission mode. The energy was calibrated by setting the first inflection point of a Fe foil to 7112 eV. Reference and sample spectra were processed and analyzed using the software code Athena.[34] The E_0 was fixed at 7126.99 eV. The spectra were normalized by subtracting a first-order polynomial fitted to the data from −150 to −30 eV before the edge and subsequently dividing through a second-order polynomial

https://doi.org/10.1021/acsearthspacechem.1c00159
ACS Earth Space Chem. 2021, 5, 2768−2777

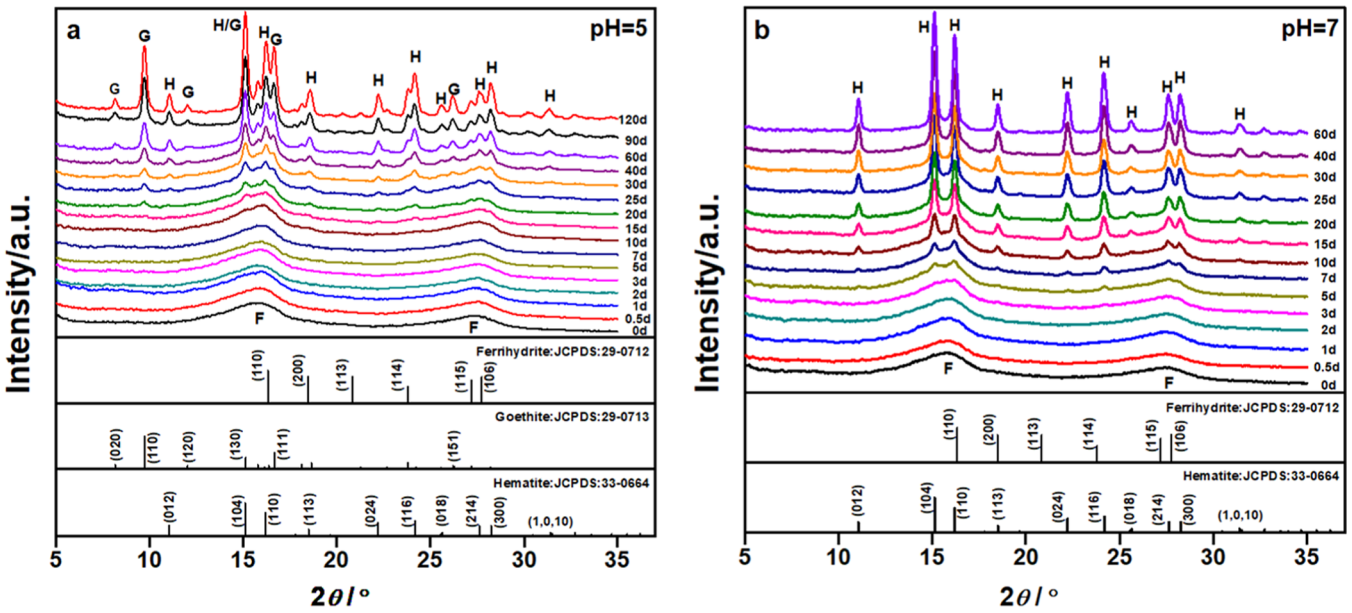

Figure 1. X-ray diffraction patterns of Fe (oxyhydr)oxide phases in the presence of REEs during aging (0−120 days) at pH 5 (a) and 7 (b).

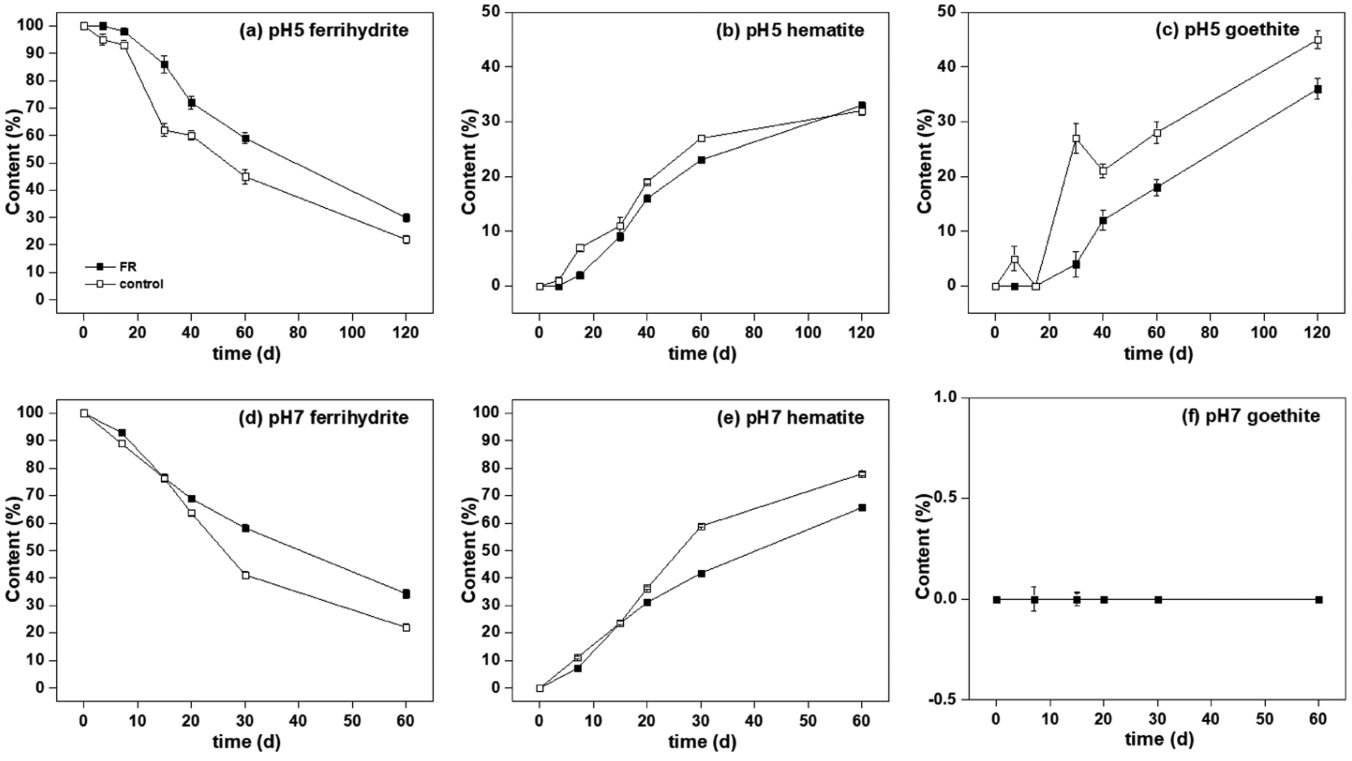

Figure 2. Linear combination fit (LCF) analysis of Fe K-edge X-ray absorption spectroscopy (XAS) spectra of aged REE-ferrihydrite (i.e., ferrihydrite coprecipitated with REEs) at pH 5 (a−c) and 7 (d−f). Closed squares represent samples with REEs (FR) and open squares represent control samples that are without REEs. The results of LCF of Fe K-edge XAS analysis are shown in Figures S2 and S3.

fitted to the data from 150 to 527 eV above the edge. The spectra were extracted using the Autobk algorithm. For the interpretation of the experimental spectra by linear combination fitting (LCF) over the *k*-range 2−10 $Å^{-1}$, three reference samples including ferrihydrite, goethite, and hematite were used (Figure S1).

Neodymium and Ytterbium Adsorption in Iron (Oxyhydr)oxides. To better understand the pH-dependent adsorption of LREEs and HREEs in the transformation products of ferrihydrite, neodymium (Nd) and ytterbium (Yb) were chosen as representative LREEs and HREEs to conduct batch adsorption experiments in ferrihydrite synthesized at pH 5 and 7, hematite, and goethite under the following reaction conditions (ionic strength: 0.01 mol L^{-1} KCl, 25 °C). These iron (oxyhydr)oxides were identified in XRD and XAS analyses. Accordingly, iron (oxyhydr)oxide stock suspensions (∼0.8 g L^{-1}) were prepared in a background electrolyte solution and then sonificated for 30 s. After 2−3 days of

https://doi.org/10.1021/acsearthspacechem.1c00159
ACS Earth Space Chem. 2021, 5, 2768−2777

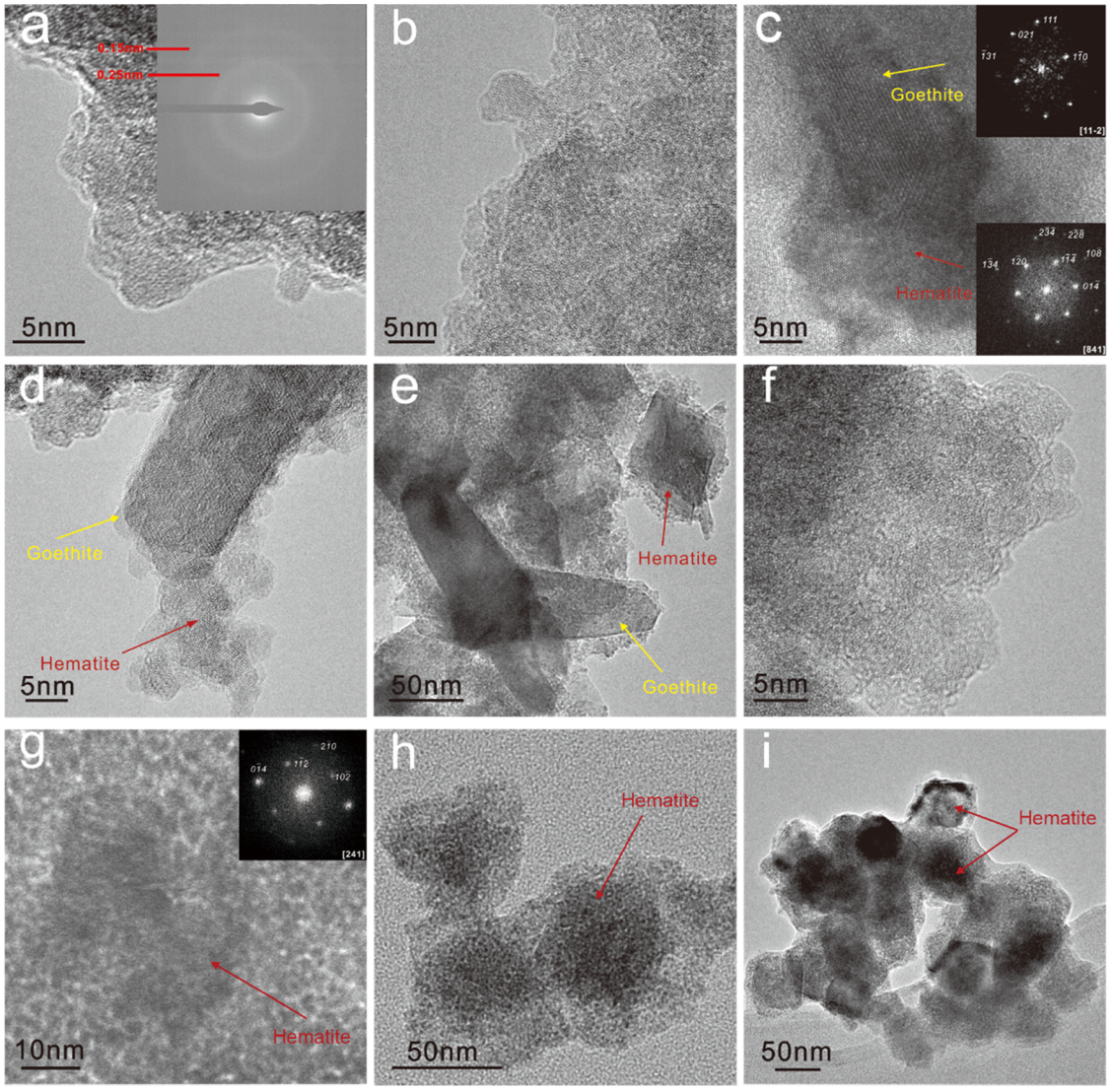

Figure 3. Transmission electron microscopy images of aged Fe (oxyhydr)oxides coprecipitated with REEs at pH 5, (a) t = 0 day, (b) 7 days, (c) 15 days, (d) 60 days, and (e) 120 days and at pH 7, (f) t = 0 day, (g) 7 days, (h) 15 days, and (i) 60 days.

hydration on an orbital shaker, ~9 mL of iron (oxyhydr)oxides suspension was transferred into a tube. pH of the suspension was adjusted to 4.0−9.0 in 0.5 pH unit increment using 0.1 mol L^{-1} HCl and NaOH. One mL of 1 mg L^{-1} Nd/Yb stock solution was added. The final volume was adjusted to 10 mL using the background electrolyte to make the final suspension density of 0.86 g L^{-1} for ferrihydrite, 0.80 g L^{-1} for goethite, and 0.71 g L^{-1} hematite. The final suspension density of goethite and hematite was based on the reaction condition of the aging experiment assuming 100% of ferrihydrite was transformed to goethite or hematite. The tubes were shaken at 200 rpm for 24 h. After equilibration, aliquots were recovered via centrifugation at 23 723g for 10 min. and then filtered through a 0.22 μm membrane filter. After acidification with 2% HNO_3, the concentrations of Nd and Yb were analyzed using ICP-MS (Thermo iCAPQc, Guangzhou, China).

ζ-Potential Measurements. ζ-Potential measurements were conducted in ferrihydrite synthesized at pH 5 and 7, hematite, and goethite using a Zetasizer Nano ZS 90 (Malvern Instruments Ltd., Malvern, U.K.). The electric field strength was approximately 3.95 V mm^{-1}. Verification of the instrument was performed using a polystyrene latex standard. A mineral suspension (0.5 g L^{-1}) was prepared in 0.01 mol L^{-1} $NaNO_3$ and sonicated. pH was adjusted to 4−9 with 0.01−0.1 M HNO_3/NaOH. After 24 h of equilibration, the ζ-potential was measured three times for each sample.

RESULTS AND DISCUSSION

The results of XRD, XAS, and TEM analyses of the transformation products are summarized in Figures 1−3 and S2−S5. To further distinguish the effect of REEs on the transformation of iron (oxyhydr)oxides, the phase composition was quantified by the LCF of Fe K-edge EXAFS analysis using ferrihydrite, goethite, and hematite (Figure 2, Tables S2, and S3).

The conditions of the transformation of ferrihydrite have been studied by Schwertmann et al.[35,36] According to their studies, the rate and degree of transformation increased with increasing pH and temperature. Especially, the value of pH is determinant for the formation of different iron (oxyhydr)-oxides. Protons or hydroxyl groups promote dissolution of Fe(III) at acidic or alkaline pH values (e.g., 2−5 and 10−14, respectively) and favor the formation of goethite through a dissolution−recrystallization process. Conversely, at near-

https://doi.org/10.1021/acsearthspacechem.1c00159
ACS Earth Space Chem. 2021, 5, 2768−2777

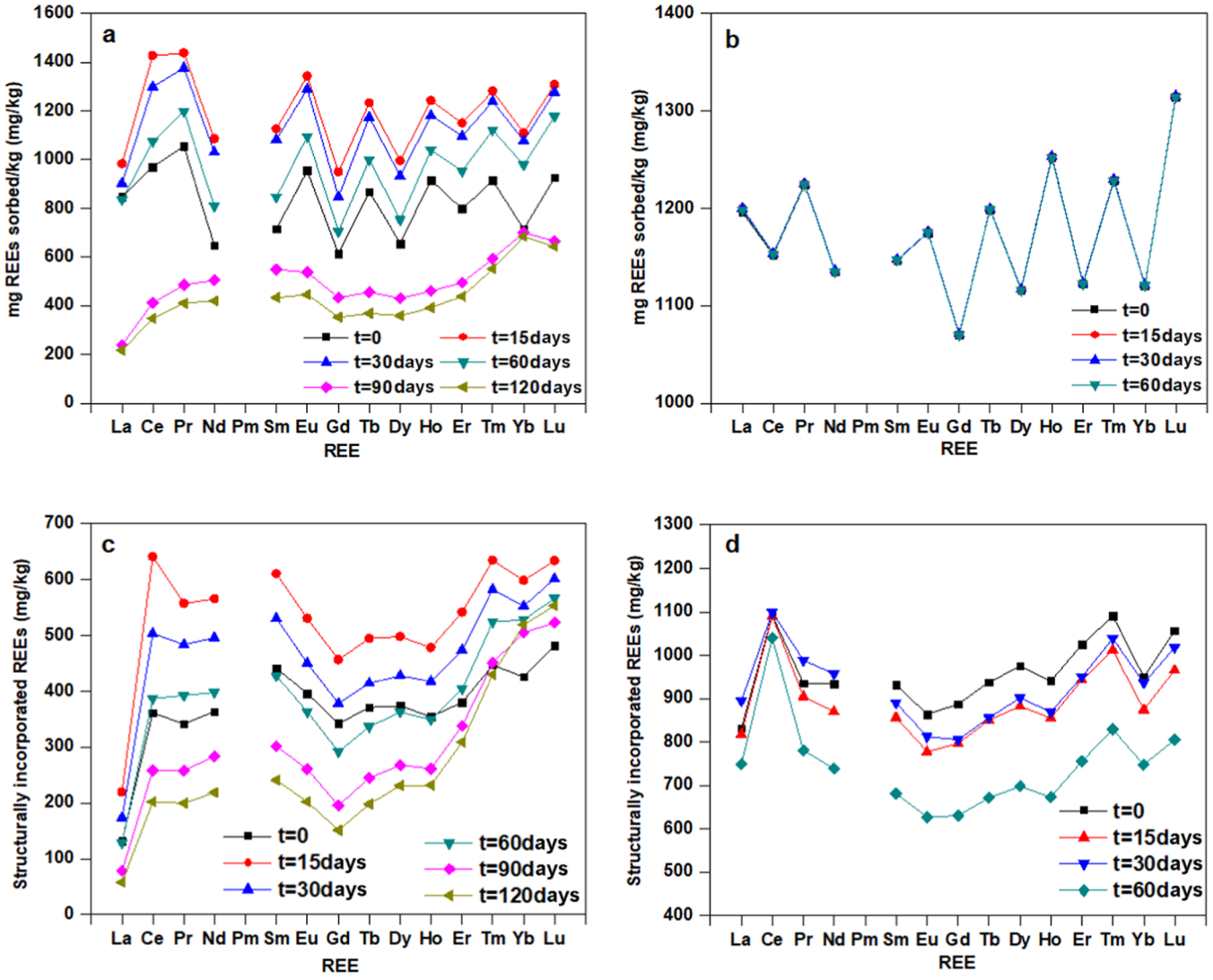

Figure 4. Total REE sorption in aged REE-ferrihydrite at (a) pH 5 and (b) pH 7. The values were calculated from the ICP-MS data. Structurally incorporated REEs in aged REE-ferrihydrite at (c) pH 5 and (d) pH 7. The values were calculated via digestion of aged samples after removal of adsorbed REEs.

neutral pH, dissolution of Fe(III) was minimum, and the condition favored the formation of hematite through a solid-state transformation process. Based on the above information, the discussion section was organized according to the experimental pH values (5 and 7) that strongly influence the transformation processes of ferrihydrite.

Transformation Products of Aged REE-Ferrihydrite at pH 5. According to the XRD analyses, the dominant mineral phase of the precipitate was two-line ferrihydrite at t=0, with board reflections at 16° (2.50 Å) and 27° (1.51 Å) (Figure 1a). The XAS analysis showed that the transformation of ferrihydrite in the presence of REEs was always slower than the system without REEs (Figure 2a). After seven days, ~5% of ferrihydrite was transformed in the absence of REEs, while the only ferrihydrite without goethite or hematite existed with REEs (Table S2). TEM images showed that the precipitates were aggregates of fine particles in the size of 2−3 nm, which exhibited two bright rings with lattice spacings of 2.5 and 1.5 Å in selected area electron diffraction (SAED),[37] corresponding to (110) and (115) planes of 2-line ferrihydrite (Figure 3a). In the absence of REEs, the Fe precipitate produced under the same condition showed identical morphology and mineral phase (Data not shown).

With increasing aging time, most Fe was insoluble (Figure S6), while the precipitate of Fe and REEs was kept as the phase of ferrihydrite until 15 days (Figure 1). Then, it was gradually transformed into goethite and hematite. This was verified by the appearance of new reflections on the XRD patterns of reaction products at 20, 25, and 30 days, i.e., (104) and (110) of hematite at 15° (2.70 Å) and 16° (2.50 Å), respectively, as well as the (110) of goethite at 10° (4.18 Å) (Figure 1).

After 60 days, the XRD patterns became well resolved and corresponded well to the standard card of hematite (JCPDS: 33-0664) and goethite (JCPDS: 29-0713). Without the presence of REEs, the transformation of ferrihydrite was mostly parallel, with similar mineral phases of end products and transformation progress, whereas the transformation rate and phase composition were slightly different. For example, the XRD patterns of ferrihydrite did not show obvious changes until 15 days of aging (Figure S1a).

Then, the diffraction at 15.5° (2.56 Å) was split into two peaks at 15° (2.70 Å) and 16° (2.50 Å), indexed of (104) and

https://doi.org/10.1021/acsearthspacechem.1c00159
ACS Earth Space Chem. 2021, 5, 2768−2777

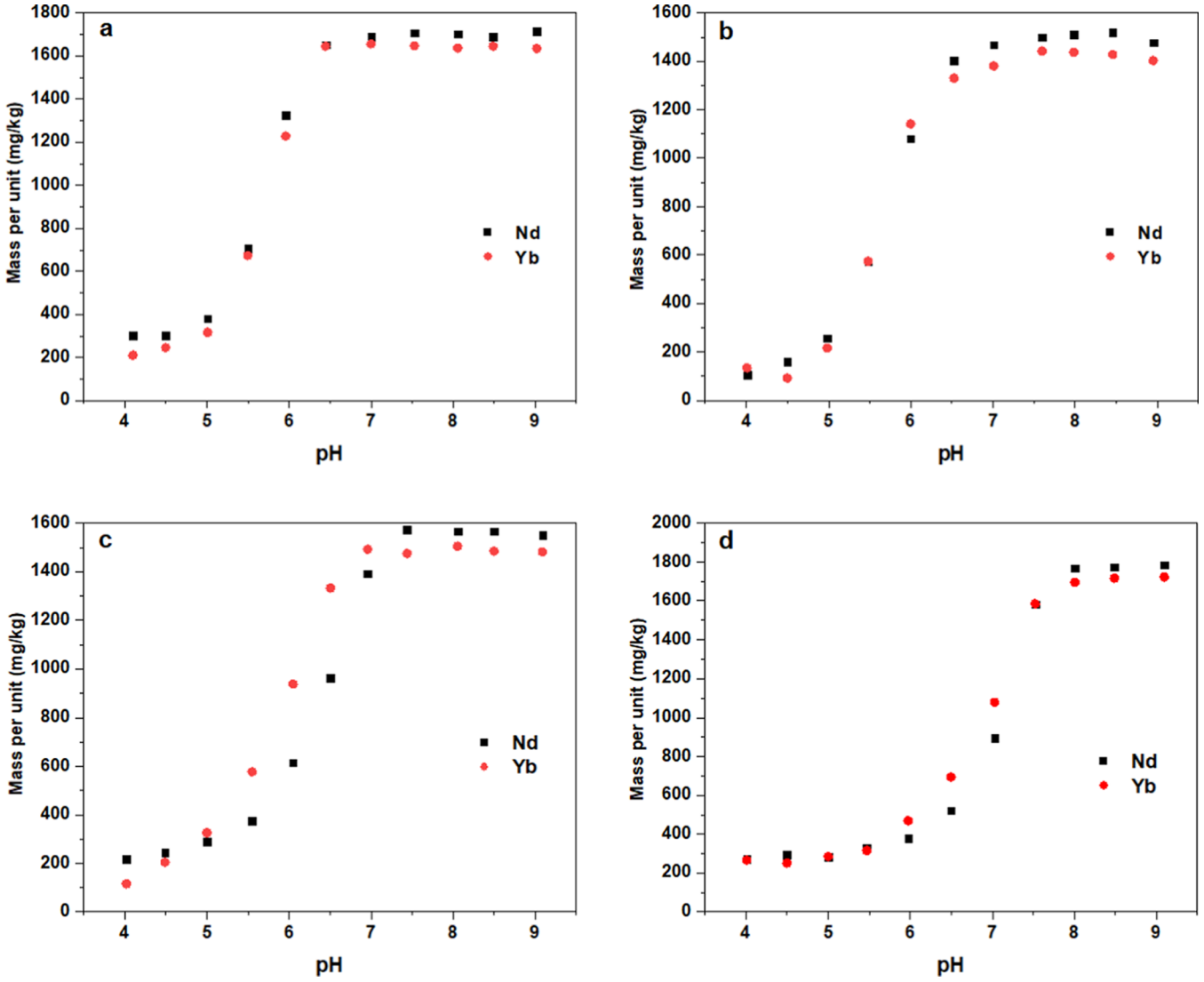

Figure 5. pH adsorption edge of Nd and Yb in ferrihydrite synthesized at pH 5 (a), ferrihydrite synthesized at pH 7 (b), goethite (c), and hematite (d).

(110) of hematite, respectively. After 20 days, the (110) diffraction of goethite appeared at 10° (4.18 Å) (2θ). However, the formation and crystallization of goethite seemed to be inhibited by the addition of REEs, since the diffraction intensity ratio of $(110)_{hematite}$ to $(111)_{goethite}$ was 0.93 without REEs, obviously lower than that with REEs (1.07).

Besides phase composition, the morphology of precipitate also greatly varied during aging with REEs. According to the TEM observation, the particle size of ferrihydrite increased from 2−3 to 5 nm within 7 days (Figure 3b). After 15 days of incubation, not only hematite that was detected by XRD but also goethite was observed (Figure 3c). Both the formations of hematite and goethite were consolidated by the fast Fourier transform (FFT) pattern (Figure 3c). The FFT image clearly displays the fringe spacings of 4.15, 2.58, 2.45, and 2.0 Å, which were consistent with the *d*-values of (110), (021), (111), and (131) reflection planes of orthorhombic goethite, respectively. For hematite, the FFT image displays spot patterns corresponding to the six sets of reflections of hematite. The absence of goethite by XRD was probably ascribed to its low content (<5%) and poor crystallinity. Goethite displayed a lath shape with particle size of 30-40 nm, while hematite with a smaller size (10−30 nm) did not show a regular shape. The conspicuous appearance of hematite and goethite was seen after 60 days (Figure 3d,e), accompanied by the increase of the particle size. Goethite and hematite displayed needle and rhombohedra shapes, with sizes of 180 and 80−90 nm, respectively (Figure 3e). In the presence of REEs, the transformation products were lath-shape goethite and rhombohedron hematite without a clear morphology (Figure S5). The length of goethite (~100 nm) was smaller than that of goethite without REEs, whereas the size of hematite was larger than its counterpart. (Figure S5). Moreover, it is necessary to mention that ferrihydrite was still found in the aged sample after 120 days. With increasing aging time to seven days, the XAS spectra feature at ~5 $Å^{-1}$ gradually changed, indicating the formation of goethite and/or hematite (Figures S1 and S3a). As the samples were aged, the content of ferrihydrite gradually decreased and achieved 30.4 and 22.2% with and without REEs, respectively, after 120 days (Figure 2 and Table S2). This suggests that the presence of REEs retarded the transformation of ferrihydrite. However, the production of hematite was not affected by the introduction of REEs, wherein both cases, ~33% was detected in the final iron

https://doi.org/10.1021/acsearthspacechem.1c00159
ACS Earth Space Chem. 2021, 5, 2768−2777

(oxyhydr)oxide composition after 120 days. As for goethite, its formation with the presence of REEs was about 10% lower than that without REEs. Therefore, REEs selectively suppressed the formation of goethite rather than hematite, which is in accord with the XRD results.

Mechanisms of REE-Suppressed Goethite Formation at pH 5. The formation of goethite was suppressed by REEs at pH 5 (Figure 2c). For goethite to form, dissolution of Fe must occur first, and this can be suppressed by REE sorption.

Figure 4 shows the concentration of REEs in solids during aging. It is important to note that the total REE sorption or partitioning in solids represents a sum of diffused, adsorbed, and structurally incorporated REE ions (Figure 4a). There was an increase in REE retention in ferrihydrite from 0 to 15 days, and then, REE retention started to decrease after 15 days. This is due to a decrease in the surface area since more crystalline phases were formed with aging (Figure 2b,c). It is possible that the aggregation of ferrihydrite also reduced the specific surface area of ferrihydrite,[38] which caused the considerable release of REEs. It is difficult to observe the trend of REE-specific retention because pH 5 is below the IEP of major iron (oxyhydr)oxides (Figure S7). The adsorption of REEs should be minimal if any adsorption occurred. Accordingly, adsorption of LREEs and HREEs was evaluated in three iron (oxyhydr)-oxides using Nd and Yb, which represent LREEs and HREEs, respectively (Figure 5). At pH 5, there was a small amount (~200−220 mg kg^{-1}) of adsorption of Nd and Yb in all of the three iron (oxyhydr)oxides.

The total sorption of REEs (~400−1100 mg kg^{-1} for Nd and ~700−1100 mg kg^{-1} for Yb) during the ferrihydrite transformation at 0−120 days (Figure 4a) cannot be explained by only the adsorption reaction. One should also consider that the structural incorporation of REEs contributes to the overall sorption of REEs (Figure 4a) at pH 5. The structurally incorporated REEs (Figure 4c) showed that ~380−480 mg kg^{-1} of REEs were already incorporated at t = 0, and the substituted REE concentration increased after 15 days. Then, REEs were released back into the solution with increasing aging time due to the transformation of ferrihydrite to goethite.

At the beginning of aging (0−60 days), most REEs were sorbed uniformly, except for the negative anomalies of La and Gd with higher covalency (Figure 4a). La^{3+} and Gd^{3+} have different electronic configurations compared to other REEs, i.e., La^{3+}:$[Xe]4f^0$ and Gd^{3+}:$[Xe]4f^7$. The 4f electrons shield the nuclear charge less effectively than electrons in other orbitals.[39] Therefore, La^{3+} with empty 4f orbital is more covalent than other REEs, while Gd^{3+} with the half-filled 4f orbital electrons is more stable than its adjacent REEs in solution. Thus, when REEs were effectively coprecipitated with Fe, La and Gd preferred to remain in solution, giving rise to the distinct La and Gd anomalies in solution.

In general, more HREEs were incorporated in the structure than LREEs after 120 days (Figure 4c). When the fractions of structurally incorporated Nd and Yb were compared (Figure 4a,c), more Yb was incorporated in the structure than Nd. After 120 days, ~200 mg kg^{-1} of Nd was incorporated (Figure 4c), which was ~50% of the total Nd (Figure 4a), while Yb in the structure was ~550 mg kg^{-1} (Figure 4c), which was ~80% of the total Yb (Figure 4a). Due to the smaller ionic radii and greater affinity of HREEs with iron (oxyhydr)oxides, more HREEs were associated with iron (oxyhydr)oxides.

Finck et al.[27] reported that Lu, one of HREEs, incorporation in hematite and goethite after Lu coprecipitated with ferrihydrite was aged for 12 years at room temperature.[27] LREEs and HREEs behaved incoherently due to the subtle difference of their effective radii and affinities to iron oxides. The ionic radii of REE(III) decrease from La^{3+} (1.032 Å, 6-coordination) to Lu^{3+} (0.861 Å, 6-coordination), which are larger than those of Fe^{3+} (0.645 Å, 6-coordination).[40] Considering the close ionic radii of HREEs to Fe, HREEs are more preferably incorporated into goethite or hematite than LREEs. In this experiment, we did not observe four upward-curved segments (I: La−Nd, II: Nd−Gd, III: Gd−Ho, IV: Ho−Lu) that were reported by Bau.[39] This is probably due to the initial concentration of REEs in this study, which was two orders of magnitude greater than Bau's study. Competitive adsorption of REEs might have also diminished the trend.

In summary, dissolution of ferrihydrite and recrystallization of Fe(III) were suppressed by both adsorption and structural incorporation of REEs at pH 5. These two reactions are equally important at pH 5. A similar phenomenon was also found with the presence of Cu^{2+}.[41] Low levels of Cu^{2+} (9 mol %) suppressed the formation of goethite by hindering the dissolution of ferrihydrite. Fei et al. also reported that La and Ho adsorption retarded the phase transformation of ferrihydrite after 60 days at room temperature.[42]

Transformation Products of Aged REE-Ferrihydrite at pH 7. Neutral pH is an optimum pH to promote the transformation of ferrihydrite to hematite. No goethite was formed in the systems at pH 7 with and without REEs (Figures 1b and S1b). At pH 7, according to XRD (Figure 1b) and TEM analyses (Figure 3f), 2−3 nm nanosized ferrihydrite was the only initial solid phase in both cases with or without REEs. In the former case, hematite began to form after 5 days, as evident in the new reflections at 15° (2.70 Å) and 16° (2.50 Å) (2θ) (Figure 1b) on the XRD patterns, corresponding to (104) and (110) planes of hematite, respectively. TEM images showed that the particle size of ferrihydrite increased from 2−3 to 10 nm in the initial 7 days. Meanwhile, the occurrence of hematite with an unclear border was also confirmed by the FFT pattern (Figure 3g), with a particle size of 40 nm. Thus, the size of ferrihydrite and hematite was larger than those (5 nm) formed at the same aging time under pH 5. With increasing aging time from 15 to 60 days, more distinguishable hematite particles appeared (Figure 3g−i). Their grains were present as a loose structure, and the size slightly grew to ca. 50 nm (Figure 3h,i). After 60 days, the XRD patterns of hematite became clearer. The rhombohedral shape of hematite was clearly observed without significant alteration of the particle size (Figure 3i). Interestingly, the diffraction peaks of hematite were sharper in control than those with REEs (Figures 1b and S1b), suggesting that REEs reduced the crystallinity of hematite. At pH 7, both transformation products contain cubic and spherical hematite and the addition did not alter the morphology of hematite (Figure S8).

As shown in XAS spectra (Figure S4a), an increase in aging time gradually changed the shape of the peak at ~5 Å, which resembles the spectrum of hematite (Figures S2 and S4). The LCF analysis showed that the transformation products were not different between the control and the system with REEs during the initial 15 days (Figure 2d). With increasing aging time to 30 days, however, the content of hematite in the solution with REEs was less than that in the solution without REEs. The content of ferrihydrite was 41.7 and 58.9% with and without REEs, respectively (Table S3), suggesting the REEs suppressed the transformation of ferrihydrite to hematite. After

https://doi.org/10.1021/acsearthspacechem.1c00159
ACS Earth Space Chem. 2021, 5, 2768−2777

60 days, the difference in hematite formation was more evident with and without REEs (Table S3). No goethite formation was observed (Figure 2f).

Mechanisms of REE-Suppressed Hematite Formation at pH 7. Both Fe and REE are easily hydrolyzed and precipitated at pH 7 from the solution. Figure S8 shows the first hydrolysis constants ($\log \beta_1$) of REEs at 25 °C and zero ionic strength, according to the study by Klungness and Byrne.[43] The $\log \beta_1$ values of REEs increase with the atomic number but show a noticeable negative Gd anomaly. The first hydrolysis constant ($\log \beta_1$) of Fe is −2.19.[44] This suggests that Fe is more hydrolytic than REEs. In fact, the dissolved Fe concentration was near negligible during aging (Figure S6).

At pH 7, according to the LCF XAS analysis, the formation of hematite was suppressed by addition of REEs (Figure 2e). The transformation from ferrihydrite to hematite requires internal aggregation and rearrangement.[41,45] At neutral pH conditions, there was a strong affinity of REEs onto ferrihydrite surfaces (Figure 4b). Figure 5 shows a strong adsorption of Nd and Yb, which represent LREEs and HREEs, respectively, in iron (oxyhydr)oxides at pH 7, which is near IEP values of all iron (oxyhydr)oxides (Figure S7). Nd and Yb adsorption in reference iron (oxyhydr)oxides was maximized to ∼1400−1700 mg kg^{-1} at pH 7 (Figure 5). Neutral pH near and or above IEP of the three iron (oxyhydr)oxides enhanced the adsorption (Figure S7). Nd and Yb adsorption at pH < IEP can be indirectly explained by the formation of inner-sphere surface complexes. This strong adsorption might support no net changes in total REE sorption with increasing aging time (Figure 4b). However, the concentration of structurally incorporated REEs changed with aging (Figure 4d). In general, there was a decreasing trend in REE structural incorporation from 30 to 60 days (Figure 4d). During the period, ferrihydrite began to transform into hematite (Figure 2d,e) and the rearrangement of REE-iron polymers led to less structural incorporation of REEs after 30 days. The change was more pronounced in HREEs, and there was a small change in the substitution of LREE (e.g., Ce). It is possible that Ce(III) was oxidized after adsorption to ferrihydrite,[21,40] contributing to the anomaly. Since K_{sp} of $Ce(IV)(OH)_4(s)$ (2.00×10^{-48})[46] is much lower than that of $Ce(III)(OH)_3(s)$ (1.6×10^{-20}), the presence of surface-catalyzed $Ce(OH)_4$ will not allow the rearrangement of iron polymers. The oxidative precipitation of $Ce(IV)(OH)_4$ (s) on iron (oxyhydr)oxides is possible. Therefore, there was no obvious change in Ce structural incorporation with aging. The accumulation of Ce was previously reported in marine hydrogenetic ferromanganese crusts.[21] Unfortunately, the Ce(IV) was not directly observed due to its low concentration in solids and in mixture with other REEs.

Light REEs (e.g., Nd(III): 0.983 Å) adsorbed on iron polymers could also obstruct the olation/aggregation of ferrihydrite particles because the ionic radii of LREE(III) are much larger than those of Fe(III) (0.645 Å) and HREEs (e.g., Lu(III): 0.861 Å).[39] Meanwhile, the adsorbed LREEs on ferrihydrite surface could lead to the structural mismatch between these nanoparticles and subsequently hinder these particles' oriented attachment, which has been demonstrated to be an important pathway for mineral growth in supergene environments.[47] In other words, LREE sorption stabilized the ferrihydrite surfaces. In fact, ∼40% of initial ferrihydrite remained after 60 days (Figure 2d). A similar stabilization effect of Cd^{2+} adsorption on ferrihydrite was reported at neutral pH.[48] The effects of Ce^{3+}, Nd^{3+}, Tb^{3+}, and Lu^{3+}adsorption are also known to stabilize ferrihydrite at pH 7 under reduced conditions.[30] Compared with the results of the pH 5 system, the total REE sorption in ferrihydrite at pH 7 was much greater, especially for LREEs. The retardation of ferrihydrite transformation was contributed mainly by the structural incorporation of both LREEs and HREEs. When fractions of structurally incorporated LREEs and HREEs were compared (Figure 4d), there was no clear trend of structural incorporation of REEs between LREEs and HREES in aged samples except for the anomaly of Ce.

CONCLUSIONS

In the present study, effects of REEs at 1 mg L^{-1} on the transformation products of ferrihydrite were investigated at pH 5 and 7. It was clear that the formation of goethite and hematite was perturbed by REEs at pH 5 and 7, respectively. The underlying mechanisms (i.e., adsorption and or structural incorporation of REEs) by which they interact with iron (oxyhydr)oxides are different, as discussed above. More importantly, REEs were readily sequestered in iron (oxyhydr)-oxides at both pH values, and more REEs were structurally incorporated in iron (oxyhydr)oxides at pH 7 than at pH 5. At pH 5, however, more HREEs were preferentially sequestered by iron (oxyhydr)oxides during the transformation process, which is of significant importance for the understanding of the incoherent behavior of REEs during the formation of secondary minerals like iron (oxyhydr)oxides in a mildly acidic environment.[22] The study provides important geochemical information, i.e., structural distribution of REEs in iron (oxyhydr)oxides, which is useful in improving the recovery technology of REEs from regolith-hosted deposits, acidic weathered soils and sediments.

ASSOCIATED CONTENT

Supporting Information

The Supporting Information is available free of charge at https://pubs.acs.org/doi/10.1021/acsearthspacechem.1c00159.

Results of LC fit of Fe K-edge EXAFS spectra, the phase composition of iron (oxyhydr)oxides, XRD data of control systems, saturation index values of REE hydroxides, hydrolysis constants of REEs, Nd and Yb adsorption edge data in iron (oxyhydr)oxides, and ζ-potential of iron (oxyhydr)oxides (PDF)

AUTHOR INFORMATION

Corresponding Authors

Hongping He − *CAS Key Laboratory of Mineralogy and Metallogeny/Guangdong Provincial Key Laboratory of Mineral Physics and Materials, Guangzhou Institute of Geochemistry, Chinese Academy of Sciences, Guangzhou 510640, P. R. China; CAS Center for Excellence in Deep Earth Science, Guangzhou 510640, P. R. China; University of Chinese Academy of Sciences, Beijing 100049, P. R. China*; Email: hehp@gig.ac.cn

Yuji Arai − *Department of Natural Resources and Environmental Sciences, University of Illinois at Urbana-Champaign, Urbana, Illinois 61801, United States*; orcid.org/0000-0002-2560-7445; Email: yarai@illinois.edu

https://doi.org/10.1021/acsearthspacechem.1c00159
ACS Earth Space Chem. 2021, 5, 2768−2777

Authors

Meijun Yang − *CAS Key Laboratory of Mineralogy and Metallogeny/Guangdong Provincial Key Laboratory of Mineral Physics and Materials, Guangzhou Institute of Geochemistry, Chinese Academy of Sciences, Guangzhou 510640, P. R. China; University of Chinese Academy of Sciences, Beijing 100049, P. R. China*

Xiaoliang Liang − *CAS Key Laboratory of Mineralogy and Metallogeny/Guangdong Provincial Key Laboratory of Mineral Physics and Materials, Guangzhou Institute of Geochemistry, Chinese Academy of Sciences, Guangzhou 510640, P. R. China; CAS Center for Excellence in Deep Earth Science, Guangzhou 510640, P. R. China; University of Chinese Academy of Sciences, Beijing 100049, P. R. China;* orcid.org/0000-0001-6674-9354

Ying Li − *Department of Natural Resources and Environmental Sciences, University of Illinois at Urbana-Champaign, Urbana, Illinois 61801, United States*

Runliang Zhu − *CAS Key Laboratory of Mineralogy and Metallogeny/Guangdong Provincial Key Laboratory of Mineral Physics and Materials, Guangzhou Institute of Geochemistry, Chinese Academy of Sciences, Guangzhou 510640, P. R. China; CAS Center for Excellence in Deep Earth Science, Guangzhou 510640, P. R. China; University of Chinese Academy of Sciences, Beijing 100049, P. R. China;* orcid.org/0000-0002-7591-6625

Complete contact information is available at: https://pubs.acs.org/10.1021/acsearthspacechem.1c00159

Notes

The authors declare no competing financial interest.

■ ACKNOWLEDGMENTS

This work was financially supported by the National Key R&D Program of China (Grant No. 2017YFC0602306); the Key Research Program of the Institute of Geology & Geophysics, CAS (Grant No. IGGCAS-201901); the National Natural Science Foundation of China (Grant Nos. 41921003 and 41773113); the Science Research Program of Guangzhou, China (Grant No. 201804020037); and the Science and Technology Planning of Guangdong Province, China (Grant Nos. 2017B030314175, 2020B1212060055, 2020B1515020015, and 2017GC010578); and the Guangdong Major Project of Basic and Applied Basic Research (Grant No. 2019B030302013). This is contribution No.IS-3058 from GIGCAS. The use of the Advanced Photon Source was supported by the U. S. Department of Energy, Office of Science, Office of Basic Energy Sciences, under Contract No. DE-AC02-06CH11357.

■ REFERENCES

(1) Planavsky, N.; Bekker, A.; Rouxel, O. J.; Kamber, B.; Hofmann, A.; Knudsen, A.; Lyons, T. W. Rare earth element and yttrium compositions of Archean and Paleoproterozoic Fe formations revisited: New perspectives on the significance and mechanisms of deposition. *Geochim. Cosmochim. Acta* **2010**, *74*, 6387−6405.

(2) Alibert, C. Rare earth elements in Hamersley BIF minerals. *Geochim. Cosmochim. Acta* **2016**, *184*, 311−328.

(3) Busigny, V.; Planaysky, N. J.; Goldbaum, E.; Lechte, M. A.; Feng, L.; Lyons, T. W. Origin of the Neoproterozoic Fulu iron formation, South China: Insights from iron isotopes and rare earth element patterns. *Geochim. Cosmochim. Acta* **2018**, *242*, 123−142.

(4) Sholkovitz, E. R. The aquatic chemistry of rare earth elements in rivers and estuaries. *Aquat. Geochem.* **1995**, *1*, 1−34.

(5) Oonk, P. B. H.; Mason, P. R. D.; Tsikos, H.; Bau, M. Fraction-specific rare earth elements enable the reconstruction of primary seawater signatures from iron formations. *Geochim. Cosmochim. Acta* **2018**, *238*, 102−122.

(6) Singh, P.; Rajamani, V. REE geochemistry of recent clastic sediments from the Kaveri floodplains, southern India: implication to source area weathering and sedimentary processes. *Geochim. Cosmochim. Acta* **2001**, *65*, 3093−3108.

(7) Thompson, A.; Amistadi, M. K.; Chadwick, O. A.; Chorover, J. Fractionation of yttrium and holmium during basaltic soil weathering. *Geochim. Cosmochim. Acta* **2013**, *119*, 18−30.

(8) Sanematsu, K.; Kon, Y.; Imai, A.; Watanabe, K.; Watanabe, Y. Geochemical and mineralogical characteristics of ion-adsorption type REE mineralization in Phuket, Thailand. *Miner. Deposita* **2013**, *48*, 437−451.

(9) Sanematsu, K.; Ejima, T.; Kon, Y.; Manaka, T.; Zaw, K.; Morita, S.; Seo, Y. Fractionation of rare-earth elements during magmatic differentiation and weathering of calc-alkaline granites in southern Myanmar. *Mineral. Mag.* **2016**, *80*, 77−102.

(10) Sanematsu, K.; Murakami, H.; Watanabe, Y.; Duangsurigna, S.; Siphandone, V. Enrichment of rare earth elements (REE) in granitic rocks and their weathered crusts in central and southern Laos. *Bull. Geol. Surv. Jpn.* **2009**, *60*, 527−558.

(11) Padrones, J. T.; Imai, A.; Takahashi, R. Geochemical behavior of rare earth elements in weathered granitic rocks in Northern Palawan, Philippines. *Resour. Geol.* **2017**, *67*, 231−253.

(12) Janots, E.; Bernier, F.; Brunet, F.; Muñoz, M.; Trcera, N.; Berger, A.; Lanson, M. Ce (III) and Ce (IV)(re) distribution and fractionation in a laterite profile from Madagascar: insights from in situ XANES spectroscopy at the Ce LIII-edge. *Geochim. Cosmochim. Acta* **2015**, *153*, 134−148.

(13) Foley, N.; Ayuso, R. REE enrichment in granite-derived regolith deposits of the Southeastern United States: prospective source rocks and accumulation processes. *Geol. Surv. Pap.* **2015**, *3*, 131−138.

(14) Sanematsu, K.; Watanabe, Y. Characteristics and genesis of ion adsorption-type rare earth element deposits. *Rev. Econ. Geol.* **2016**, *18*, 55−79.

(15) Compton, J. S.; White, R. A.; Smith, M. Rare earth element behavior in soils and salt pan sediments of a semi-arid granitic terrain in the Western Cape, South Africa. *Chem. Geol.* **2003**, *201*, 239−255.

(16) Sultan, K.; Shazili, N. A. Rare earth elements in tropical surface water, soil and sediments of the Terengganu River Basin, Malaysia. *J. Rare Earths* **2009**, *27*, 1072−1078.

(17) Bolanz, R. M.; Kiefer, S.; Göttlicher, J.; Steininger, R. Hematite (α-Fe2O3)−A potential Ce4+ carrier in red mud. *Sci. Total Environ.* **2018**, *622*−*623*, 849−860.

(18) Quinn, K. A.; Byrne, R. H.; Schijf, J. Sorption of yttrium and rare earth elements by amorphous ferric hydroxide: Influence of solution complexation with carbonate. *Geochim. Cosmochim. Acta* **2006**, *70*, 4151−4165.

(19) Quinn, K. A.; Byrne, R. H.; Schijf, J. Sorption of yttrium and rare earth elements by amorphous ferric hydroxide: Influence of temperature. *Environ. Sci. Technol.* **2007**, *41*, 541−546.

(20) Liu, H.; Pourret, O.; Guo, H.; Bonhoure, J. Rare earth elements sorption to iron oxyhydroxide: Model development and application to groundwater. *Appl. Geochem.* **2017**, *87*, 158−166.

(21) Bau, M.; Koschinsky, A. Oxidative scavenging of cerium on hydrous Fe oxide: Evidence from the distribution of rare earth elements and yttrium between Fe oxides and Mn oxides in hydrogenetic ferromanganese crusts. *Geochem. J.* **2009**, *43*, 37−47.

(22) Lara, M. C.; Buss, H. L.; Pett-Ridge, J. C. The effects of lithology on trace element and REE behavior during tropical weathering. *Chem. Geol.* **2018**, *500*, 88−102.

(23) Dardenne, K.; Schäfer, T.; Lindqvist-Reis, P.; Denecke, M.; Plaschke, M.; Rothe, J.; Kim, J. Low temperature XAFS investigation

on the lutetium binding changes during the 2-line ferrihydrite alteration process. *Environ. Sci. Technol.* **2002**, *36*, 5092−5099.
(24) Crawford, R. J.; Harding, I. H.; Mainwaring, D. E. Adsorption and Coprecipitation of Single Heavy Metal Ions onto the Hydrated Oxides of Iron and Chromium. *Langmuir* **1993**, *9*, 3050−3056.
(25) Jang, J. H.; Dempsey, B. A.; Catchen, G. L.; Burgos, W. D. Effects of Zn(II), Cu(II), Mn(II), Fe(II), NO3-, or SO42- at pH 6.5 and 8.5 on transformations of hydrous ferric oxide (HFO) as evidenced by Mossbauer spectroscopy. *Colloids Surf., A* **2003**, *221*, 55−68.
(26) Hansel, C. M.; Learman, D. R.; Lentini, C. J.; Ekstrom, E. B. Effect of adsorbed and substituted Al on Fe(II)-induced mineralization pathways of ferrihydrite. *Geochim. Cosmochim. Acta* **2011**, *75*, 4653−4666.
(27) Finck, N.; Bouby, M.; Dardenne, K. Fate of Lu (III) sorbed on 2-line ferrihydrite at pH 5.7 and aged for 12 years at room temperature. I: insights from ICP-OES, XRD, ESEM, AsFlFFF/ICP-MS, and EXAFS spectroscopy. *Environ. Sci. Pollut. Res.* **2019**, *26*, 5238−5250.
(28) Yokosawa, T.; Prestat, E.; Polly, R.; Bouby, M.; Dardenne, K.; Finck, N.; Haigh, S. J.; Denecke, M. A.; Geckeis, H. Fate of Lu (III) sorbed on 2-line ferrihydrite at pH 5.7 and aged for 12 years at room temperature. II: Insights from STEM-EDXS and DFT calculations. *Environ. Sci. Pollut. Res.* **2019**, *26*, 5282−5293.
(29) Fei, Y.; Hua, J.; Liu, C.; Li, F.; Zhu, Z.; Xiao, T.; Chen, M.; Gao, T.; Wei, Z.; Hao, L. Aqueous Fe (II)-induced phase transformation of ferrihydrite coupled adsorption/immobilization of rare earth elements. *Minerals* **2018**, *8*, No. 357.
(30) Hua, J.; Liu, C.; Li, F.; Zhu, Z.; Wei, Z.; Chen, M.; Gao, T.; Qiu, G. Effects of rare earth elements' physicochemical properties on their stabilization during the Fe(II)(aq)-induced phase transformation of ferrihydrite. *ACS Earth Space Chem.* **2019**, *3*, 895−904.
(31) Gustafsson, J. P. *Visual MINTEQ*, version 3.1; KTH, Department Of Land and Water Resources Engineering: Stockholm, Sweden, 2020.
(32) Schwertmann, U.; Cornell, R. M. *Iron Oxides in the Laboratory: Preparation and Characterization*; John Wiley & Sons, 2008.
(33) Yang, D.; Xiao, G. Regional metallogenic regularities of the ion adsorption type of rare-earth deposits in Guangdong province. *Geol. Resour.* **2011**, *6*, 462−468.
(34) Ravel, B.; Newville, M. ATHENA, ARTEMIS, HEPHAESTUS: data analysis for X-ray absorption spectroscopy using IFEFFIT. *J. Synchrotron Radiat.* **2005**, *12*, 537−541.
(35) Schwertmann, U.; Murad, E. Effect of pH on the formation of goethite and hematite from ferrihydrite. *Clays Clay Miner.* **1983**, *31*, 277−284.
(36) Schwertmann, U.; Stanjek, H.; Becher, H.-H. Long-term in vitro transformation of 2-line ferrihydrite to goethite/hematite at 4, 10, 15 and 25 C. *Clay Miner.* **2004**, *39*, 433−438.
(37) Janney, D. E.; Cowley, J. M.; Buseck, P. R. Transmission electron microscopy of synthetic 2-and 6-line ferrihydrite. *Clays Clay Miner.* **2000**, *48*, 111−119.
(38) Stegemeier, J.; Reinsch, B.; Lentini, C.; Dale, J.; Kim, C. Aggregation of nanoscale iron oxyhydroxides and corresponding effects on metal uptake, retention, and speciation: II. Temperature and time. *Geochim. Cosmochim. Acta* **2015**, *148*, 113−129.
(39) Bau, M. Scavenging of dissolved yttrium and rare earths by precipitating iron oxyhydroxide: Experimental evidence for Ce oxidation, Y-Ho fractionation, and lanthanide tetrad effect. *Geochim. Cosmochim. Acta* **1999**, *63*, 67−77.
(40) Shannon, R. D. Revised effective ionic radii and systematic studies of interatomic distances in halides and chalcogenides. *Acta Crystallogr., Sect. A: Cryst. Phys., Diffr., Theor. Gen. Crystallogr.* **1976**, *32*, 751−767.
(41) Cornell, R.; Giovanoli, R. The influence of copper on the transformation of ferrihydrite ($5Fe_2O_3 \cdot 9H_2O$) into crystalline products in alkaline media. *Polyhedron* **1988**, *7*, 385−391.
(42) Fei, Y.; Hua, J.; Liu, C.; Li, F.; Zhu, Z.; Xiao, T.; Chen, M.; Gao, T.; Wei, Z.; Hao, L. Aqueous Fe(II)-Induced phase transformation of ferrihydrite coupled adsorption/immobilization of rare earth elements. *Minerals* **2018**, *8*, No. 357.
(43) Klungness, G. D.; Byrne, R. H. Comparative hydrolysis behavior of the rare earths and yttrium: the influence of temperature and ionic strength. *Polyhedron* **2000**, *19*, 99−107.
(44) Stefánsson, A. Iron (III) hydrolysis and solubility at 25 C. *Environ. Sci. Technol.* **2007**, *41*, 6117−6123.
(45) Fischer, W.; Schwertmann, U. The formation of hematite from amorphous iron (III) hydroxide. *Clays Clay Miner.* **1975**, *23*, 33−37.
(46) Dahle, J. T.; Arai, Y. Environmental geochemistry of cerium: applications and toxicology of cerium oxide nanoparticles. *Int. J. Environ. Res. Public Health* **2015**, *12*, 1253−1278.
(47) Penn, R. L.; Banfield, J. F. Imperfect oriented attachment: dislocation generation in defect-free nanocrystals. *Science* **1998**, *281*, 969−971.
(48) Lin, X. M.; Burns, R. C.; Lawrance, G. A. Effect of cadmium(II) and anion type on the ageing of ferrihydrite and its subsequent leaching under neutral and alkaline conditions. *Water, Air, Soil Pollut.* **2003**, *143*, 155−177.

https://doi.org/10.1021/acsearthspacechem.1c00159
ACS Earth Space Chem. 2021, 5, 2768−2777